Reducing Defects in Halide Perovskite Nanocrystals for Light-Emitting Applications

Xiaopeng Zheng, Yi Hou, Hong-Tao Sun, Omar F. Mohammed, Edward H. Sargent, and Osman M. Bakr

Reducing Defects in Halide Perovskite Nanocrystals for Light-Emitting Applications

Xiaopeng Zheng[1§], Yi Hou[2§], Hong-Tao Sun[3], Omar F. Mohammed[1], Edward H. Sargent[2]* and Osman M. Bakr[1]*

[1]Division of Physical Sciences and Engineering, King Abdullah University of Science and Technology (KAUST), Thuwal 23955-6900, Kingdom of Saudi Arabia

[2]Department of Electrical and Computer Engineering, University of Toronto, 10 King's College Road, Toronto, Ontario, M5S 3G4, Canada

[3]College of Chemistry, Chemical Engineering and Materials Science, Soochow University, Suzhou 215123, China

[§] These authors contributed equally.

Abstract

The large specific surface area of halide perovskite nanocrystals (NCs) increases the likelihood of surface defects compared to that in the case of polycrystalline films and single crystals. To exploit the potential of halide perovskite NCs, it is important to understand and control their defect population. This Perspective describes and classifies recent advances in understanding defect chemistry and avenues toward defect density reduction in perovskite NCs, and it does so in the context of the promise perceived in light-emitting devices. Several pathways for decreasing the defect density are explored, including advanced NC syntheses, new surface-capping strategies, doping with metal ions and rare earths, engineering elemental compensation, and the translation

of core-shell heterostructures into the perovskite materials family. We close with challenges that remain in perovskite NC defect research.

TOC Graphic

APbX$_3$ Nanocrystal

Defect Reduction
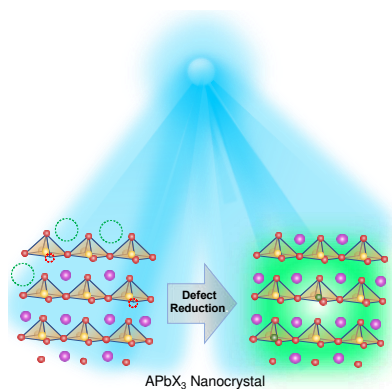
Colloidal perovskite nanocrystals (NCs) with high photoluminescence quantum yields (PLQYs), narrow emission linewidths, and tunable bandgaps are emerging as a new technology for light-emitting ~~devices~~ applications such as displays, light-emitting diodes (LEDs), and scintillators.[1-9] The external quantum efficiencies (EQEs) for both green- and red--LEDs have surpassed 20%, and the scintillators based on perovskite NCs are highly sensitive, with a detection limit lower than the typical medical imaging doses.[3, 10-13] Perovskite NCs benefit from an ionic structure and low crystallization temperature, and thus are readily synthesized via low-cost solution processes, and the ~~photoluminescence (PL)~~light-emitting wavelength is tunable from the ultraviolet (UV) to near-infrared (NIR), promising for achieving Rec. 2020 standard by changing halide composition or NC size.[14-16] The resulting perovskite NC inks allow for multiple thin-film processing methods such as spin-coating and large-area roll-to-roll printing, which are potentially compatible with the procedures developed by display manufacturers (e.g., Sony, Samsung, and LG) for CdSe- or InP-based NCs to achieve ~~fast,~~ scalable ~~, large area,~~ and ~~cost-effective~~economic panel ~~production~~manufactoring.[17-19]

Studies of the exciton binding energy (E_B) in 3D perovskites (MAPbI$_3$ and MAPbBr$_3$) reveal relatively small values varying from 2 meV to 80 meV at room temperature, and the small-E_B characteristic of 3D perovskites render them non-excitonic materials, which is beneficial to solar cells but detrimental to light-emitting applications.[20-22] By utilizing NCs, one may achieve spatial confinement of electrons and holes within a limited volume of the NCs, and increase thereby the E_B and promote radiative recombination rates, which is a crucial advantage of NCs over large-grain-sized polycrystalline films for light-emitting applications.[23-25] Although previous efforts have aimed to reduce the grain size in polycrystalline films by introducing ligands into the perovskite precursor, perovskite NCs are a very mature system, offering tunable NC sizes reaching

down to the quantum scale and abundant ligand-exchanging prototypes.[1, 12, 26] However, the trap state density is higher in NCs than in polycrystalline films/single-crystals because of the dramatically increased surface area for dangling bonds, which traps a fraction of carriers without emitting light and thus imposes severe limitations on device performance.[27-28] To enhance radiative recombination rates and reduce nonradiative ones induced by defect states, many efforts have been made to engineer these defects by removing or filling trap states in perovskite NCs. Despite ~~significant research effort~~intensive efforts, ~~many of the~~ the details of ~~finer details of~~ defect passivation mechanisms for perovskite NCs remain unclear. It is therefore necessary to summarize the existing strategies for passivating defects in perovskite NCs to further improve light-emitting devices ~~based on~~using perovskite NCs. Here, we critically review the advances made in understanding of defect passivation rules, summarize the passivation strategies for perovskite NCs, and provide a perspective on avenues for making further progress.

In 2015, Protesescu et al. synthesized ~~nearly~~ monodisperse CsPbX$_3$ (X = Cl, Br, and I) nanocubes with high ~~photoluminescence quantum yield~~PLQYs~~, suggesting a major opportunity to employ this family of materials for LEDs~~.[29] In short, CsPbX$_3$ NPs were obtained by a hot injection method in which ~~injecting~~ Cs-oleate was injected into a hot solution (140−200 °C) of PbX$_2$ (X= Cl, Br, I) salts ~~which served as a source of both Pb^{2+} and X$^−$~~ dissolved in octadecene, carboxylic acids, and primary amines. With equal ratios of amines and acids, the hot-injection method leads to the ~~formation~~harvesting of monodisperse NPs whose size can be ~~adjusted~~tuned by ~~varying~~changing both the reaction temperature and thermodynamic equilibrium. Dong et al. demonstrated ~~that it is possible~~the strategy to finely control the size of such NPs to yield ultra-high ~~ensemble~~ uniformity by operating under thermodynamic equilibrium instead of kinetic control (Figure 1a).[30]

The effect of reaction temperatures between 180 and 250 °C on $CsPbCl_3$ and $CsPbBr_3$ NCs was investigated by Dutta et al. At ~~higher temperature (~~250 °C~~)~~, a quick phase change was observed ~~to occur instantly~~, and the PLQY was dramatically enhanced. It was observed that at low temperature (<160 °C), ammonium ions competed with Cs for the A sites of the perovskite crystals and preferentially led to 2D layered perovskites as well as 3D perovskites.[31] With a further increase in reaction temperature (160-220 °C), a mixture of cubes and 2D platelets (3D perovskite) was formed; however, at 240 °C, cubes of $CsPbCl_3$ were exclusively formed. It is believed that an alkylammonium ion ~~occupies~~ takes place of the surface Cs atoms of the ~~nanocrystals~~ NCs ~~and is bound through~~ because of H-bonding with the surface halides. The presence of excess halide ions also ~~protected the nanocrystals from~~ prevented halide leaching during annealing. The powder XRD pattern of $CsPbBr_3$ NCs showed that the phase transitioned to a tetragonal phase for the reaction without ammonium chloride salts but remained in the orthorhombic phase ~~in the presence of~~ with oleylammonium salt. The wide-band-gap $CsPbCl_3$ NCs, which were reported to be poorly emissive compared with $CsPbBr_3$, could achieve an absolute quantum yield of ~51%.[32] $CuCl_2$ has been applied as an additive for high temperature synthetic protocols to yield high quality $CsPbCl_3$ NCs. The resulted NCs ~~did not~~ without show~~ing~~ ~~any~~ further PL intensity ~~enhancement~~ increasement after post-synthesis metal chloride ~~addition~~ treatment. In contrast, ~~significant~~ giant enhancement of the PL intensity was ~~observed~~ shown for pristine $CsPbCl_3$ after post-synthesis metal chloride treatment, indicating that ~~the~~ adding of $CuCl_2$ ~~assisted high temperature reaction~~ minimized the chloride deficiency (i.e. reduced Cl- vacancies) in the NCs.[33]

NCs containing only Br or I have exhibited high PLQYs of over 90 %, whereas ~~the mixed halides~~ Cl-containing $CsPbBr_xCl_{3-x}$ (x ≥ 2) ~~have~~ has shown ~~considerably~~ lower PLQYs of only 10–25 % (Figure 1b).[34] For mixed-halide perovskites, the exciton dynamics show a ~~very dissimilar~~

severe nonradiative recombination process ~~because of the~~arising from deep trap~~s energy levels~~ ~~caused~~induced by Cl vacancies (V_{Cl})~~, which lead to severe nonradiative recombination~~.[35] Moreover, the defect formation energies ~~associated with lead iodide vacancies~~ are highly sensitive to composition. In $FAPbI_3$, this energy is ~~remarkably~~ low (~0.25 eV), but ~~, corresponding to an equilibrium PbI_2 vacancy density of ~3×10^{17} cm^{-3}. W~~for the mixed- cation and -halide composition~~hen FA and I are partially replaced with Cs/MA and Br, respectively~~, the PbI_2 vacancy formation energy ~~increases more than threefold~~is much higher~~, corresponding to a reduction in the vacancy concentration by an estimated factor of 10^9~~. [36]

Liu et al. ~~prepared~~ synthesized $CsPbBr_3$ ~~NPs~~ NCs under halide-rich conditions in which ~~$PbBr_2$ was replaced with~~ PbO and NH_4Br was used to replace of $PbBr_2$ (Figure 1c). Passivating the defects with the lowest formation energy, halide vacancies, during NP synthesis under halide-rich conditions, were found to be beneficial for obtaining high PLQYs and ~~remarkable~~ enhancement of stability against purification ~~compared with those qualities achieved by conventional methods using lead halide~~.[37] LED devices fabricated with NPs synthesized under halide-rich conditions demonstrated better performance than devices containing NPs synthesized under halide-poor conditions. An LED containing $CsPbBr_3$ NPs in a 1:4 Pb:Br ratio ~~showed~~ yielded a ~~distinctly~~ improved ~~maximum~~ luminance of 12090 cd m^{-2}, a current efficiency of 3.1 cd A^{-1}, and an ~~external quantum efficiency~~EQE of 1.194%.
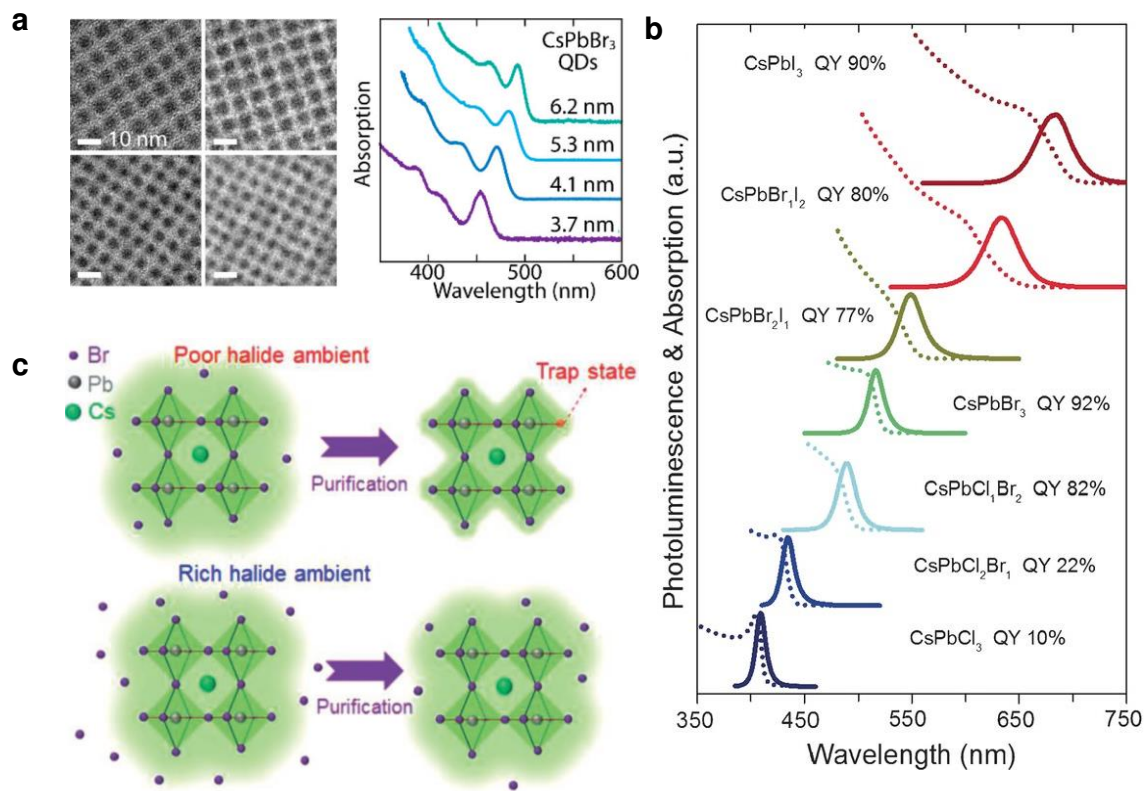
Figure 1. a. Controlling the size of CsPbX$_3$ NPs ~~with high ensemble uniformity~~ by thermodynamic equilibrium. Adapted from ref 30. Copyright 2018 American Chemical Society. **b.** UV−Vis, ~~and~~ PL spectra, and PLQYs of ~~colloidal dispersions of~~ CsPbX$_3$ NCs with different halide (X=Cl, Br, and I) compositions ~~in hexane~~. Dashed and solid lines represent for UV−Vis and PL spectra, respectively. Adapted from ref 34. Copyright 2016 Wiley‑VCH. **c.** Schematics of halide-poor and halide-rich conditions for ~~NPs~~NCs ~~(inset: NPs synthesized in a 1:4 Pb/Br solution)~~. Adapted from ref 37. Copyright 2017 American Chemical Society.

Although CsPbX$_3$ ~~NPs~~ NCs ~~synthesized by the hot injection method~~ exhibit exceptionally tunable optical properties and high PLQYs, these long-chain, insulating ligands create an unfavorable electronic energy barrier and impede electronic coupling between particles, thus limiting charge transport in devices. Usually, these long, insulating ligands are necessary for the

processing and defect passivation of the ~~NPs~~NCs. Replacing these long ligands ~~[usually oleylamine (OAm) and oleic acid]~~ with shorter ligands without ~~degrading or~~ destabilizing NP films and discovering efficient defect-passivating ligands remain the key challenges ~~preventing the fabrication of~~for efficient LEDs.

To overcome these limitations, Pan et al. developed a post-synthesis passivation process for CsPbI$_3$ NCs ~~by~~ using a bidentate ligand (~~, namely~~ 2,2′-iminodibenzoic acid (IDA)) (Figure 2a).[38] The passivated NCs exhibited narrow red ~~photoluminescence~~ PL with exceptional ~~quantum yield~~PLQY ~~(close to unity)~~ and substantially improved stability. Additionally, the passivated NCs enabled the fabrication of red LEDs with an EQE of 5.02% and a luminance of 748 cd/m^2. The passivated NCs also exhibit substantially improved environmental stability. The PL emission of untreated NCs was almost completely quenched after 5 days. In contrast, IDA-treated NCs maintained a PLQY of over 90% even after 15 days.

Due to the strong coordination ability of the P=O group, Wu et al. reported that TOPO can be a capping ligand to stabilize inorganic halide perovskite NCs.[39] They demonstrated that CsPbBr$_3$ NCs exhibited much better performance after TOPO treatment than after ethanol treatment. Similarly, by introducing the organo-lead compound trioctylphosphine−PbI$_2$ (TOP−PbI$_2$) as the reactive precursor, Liu et al. also obtained a high room-temperature PLQY of up to 100% in CsPbI$_3$ NPs, leading to significantly improved stability for the resulting CsPbI$_3$ NP solutions. Octylphosphonic acid (OPA) could also be applied to exchange the capping ligands (OA/OLA) absorbed on the perovskite NCs during synthesis. The OPA-capped CsPbX$_3$ NCs not only preserved their high PLQY (>90%) but also achieved high-quality dispersion in solvents after multiple purification processes. A green LED based on OPA-CsPbX$_3$ showed a current efficiency of 18.13 cd A^{-1} and an EQE of 6.5%.[40]

Another effective strategy has been developed by using peptides with amino and carboxylic functional groups as passivating ligands (Figure 2b).[41] When both amino and carboxylic functional groups were mixed together, ammonium moieties, $R-NH_3^+$, were generated due to the synergistic effect between the amino and carboxylic groups. This strategy proved functional for several peptides of different lengths for $CH_3NH_3PbBr_3$ as well as $CsPbBr_3$ PNCs. Peptide-based PNCs with a tunable size (~3.9 to 8.6 nm) prepared by adjusting the concentration of the peptide show size-dependent optical properties due to the quantum confinement effect.

Using a relatively short ligand, the Bakr group realized highly stable films of $CsPbX_3$ NPs capped with a halide ion pair [e.g., di-dodecyl dimethyl ammonium bromide (DDAB)], which facilitated carrier transport in quantum dot (QD) films and ultimately enabled the fabrication of efficient LEDs (Figure 2c).[42-43] The synthesis of these films was only possible through the design of a ligand-exchange strategy that includes an intermediate step to desorb protonated OAm, which otherwise would result in the degradation of all-organic QDs through a direct conventional ligand-exchange route. As a result of the novel ligand-exchange strategy, green LEDs with a maximum EQE and luminance of 3.0% and 330 cdm^{-2}, respectively, were obtained. Furthermore, the application of a similar treatment to fabricate blue LEDs resulted in a maximum EQE and luminance of 1.9% and 35 cdm^{-2}, respectively.

Similarly, Imran et al. reported a new colloidal synthesis method for preparing shape-pure and nearly monodisperse $CsPbBr_3$ nanocubes using secondary amines.[44] Regardless of the length of the alkyl chains, the oleic acid concentration, or the reaction temperature, only cube-shaped NCs were obtained. The shape purity and narrow size distribution of the nanocubes were evident from their sharp excitonic features and their ease of self-assembly in superlattices, reaching lateral dimensions of up to 50 μm. The authors attribute this excellent shape and phase purity to the

inability of secondary amines to settle into the right steric conditions at the surface of the NCs, which limits the formation of low-dimensional structures.

By using short conductive aromatic ligands, Vickers et al. reported that methylammonium lead bromide QDs prepared using benzylamine (BZA) and benzoic acid (BA) capping ligands allowed for the delocalization of the electronic wave function from the PQDs, which, in turn, facilitated charge transport between the PQDs.[45] The optimized BZA-BA-MAPbBr$_3$ QDs were highly stable and showed a very high PLQY of 86%. In addition, the BZA-BA-MAPbBr$_3$ QD film exhibited a longer carrier lifetime and more efficient charge extraction than PQDs with insulating ligands, as indicated by electrochemical measurements and transient photocurrent and photovoltage spectroscopy.

The processing and optoelectronic applications of perovskite nanocrystals are usually hampered by the loss of colloidal stability and structural integrity due to the facile desorption of surface-capping molecules during isolation and purification. To address this issue Krieg et al. proposed a new ligand-capping strategy utilizing commercially available long-chain zwitterionic molecules such as 3-(N,N-dimethyloctadecylammonio)-propanesulfonate, resulting in much stronger adhesion to the NC surface due to the chelate effect (Figure 2d).[46] This class of ligands allowed for the isolation of clean NCs with PLQYs exceeding 90% after four rounds of precipitation/redispersion along with much higher overall reaction yields of uniform and colloidal dispersible NPs. Consequently, the NCs exhibited photoconductivity and a low threshold for amplified spontaneous emission of 2 μJcm^{-2} under femtosecond optical excitation.

Lee et al. reported significant beneficial effects using a new treatment incorporating amine-based passivating materials (APMs) to passivate the defect sites of methylammonium lead tribromide through coordinate bonding between the nitrogen and undercoordinated lead ions

(Figure 2e). APM treatment resulted in enhanced PL intensity with a lower threshold for amplified spontaneous emission, a long PL lifetime, and reduced PL blinking, ultimately leading to enhanced device performance with an EQE of 6.2%. In particular, ethylenediamine (EDA) could effectively passivate defect sites in $MAPbBr_3$ on both the surface and the inside of the $MAPbBr_3$ crystal. Using confocal microscopy, the authors also observed the cessation of PL blinking in perovskite films treated with EDA due to passivation of the defect sites in $MAPbBr_3$.[47]

The anionic X-type ligands can produce trap-free bandgaps with a proposed passivation mechanism whereby new ligands bind surface lead by substituting surface halide vacancy sites, thus raising the energy of lead 6p levels to where they no longer manifest in the bandgap. X-type ligands passivate under-coordinated lead atoms, raising the absolute QYs to near unity, which indicates full trap passivation.[48]

A summary of the ligands applied for surface passivation of perovskite NCs was shown in Figure 3.
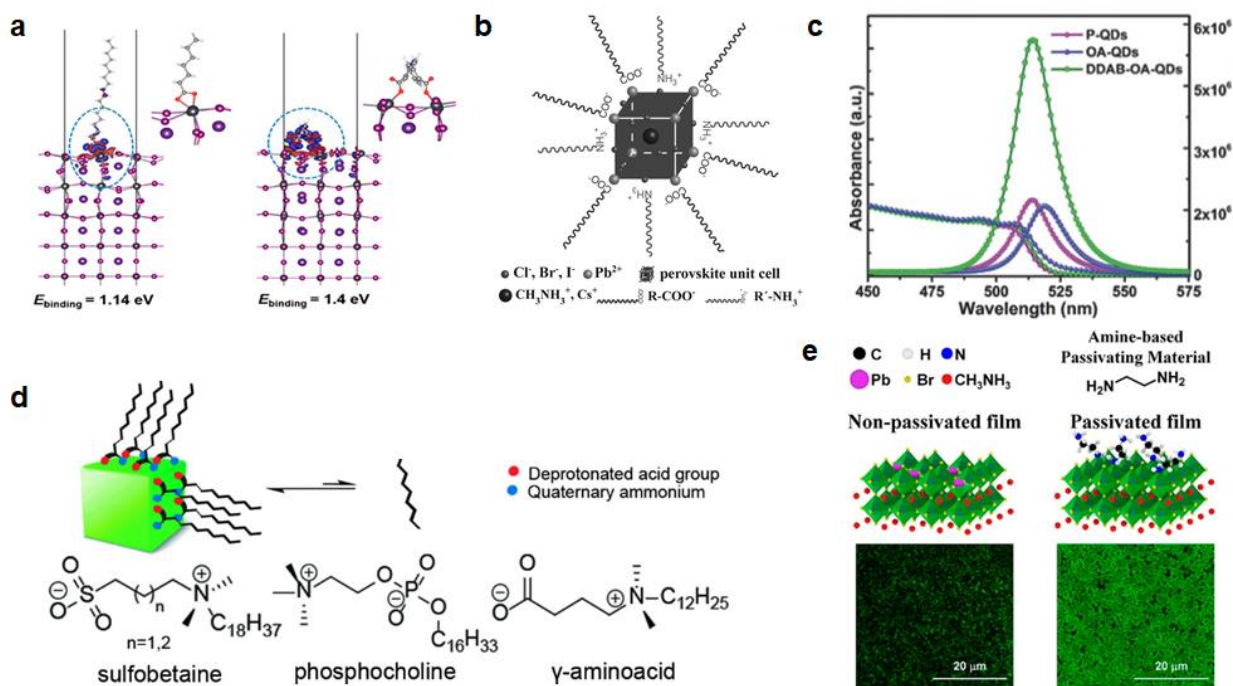
Figure 2. a. Surface charge redistributions of optimized PbI$_2$-rich CsPbI$_3$ surfaces with OA and IDA bidentate ligand modification. Adapted from ref 38. Copyright 2017 American Chemical Society. **b.** Schematic diagram illustrating the surface passivation mechanism using peptides with amino and carboxylic functional groups. Adapted from ref 41. Copyright 2017 Wiley‑VCH. **c.** UV–Vis absorption and PL spectra and FTIR spectra of purified QDs (P‑QDs), OA‑QDs, and DDAB‑OA‑QDs. Adapted from ref 42. Copyright 2016 Wiley‑VCH. **d.** Schematic diagram illustrating zwitterionic capping ligands: long-chain sulfobetaines, phosphocholines, and γ-amino acids. Adapted from ref 46. Copyright 2018 American Chemical Society. **e.** Confocal PL images and variations in PL intensities observed over time for MAPbBr$_3$ materials with and without amine-based passivating materials. Adapted from ref 47. Copyright 2017 American Chemical Society.

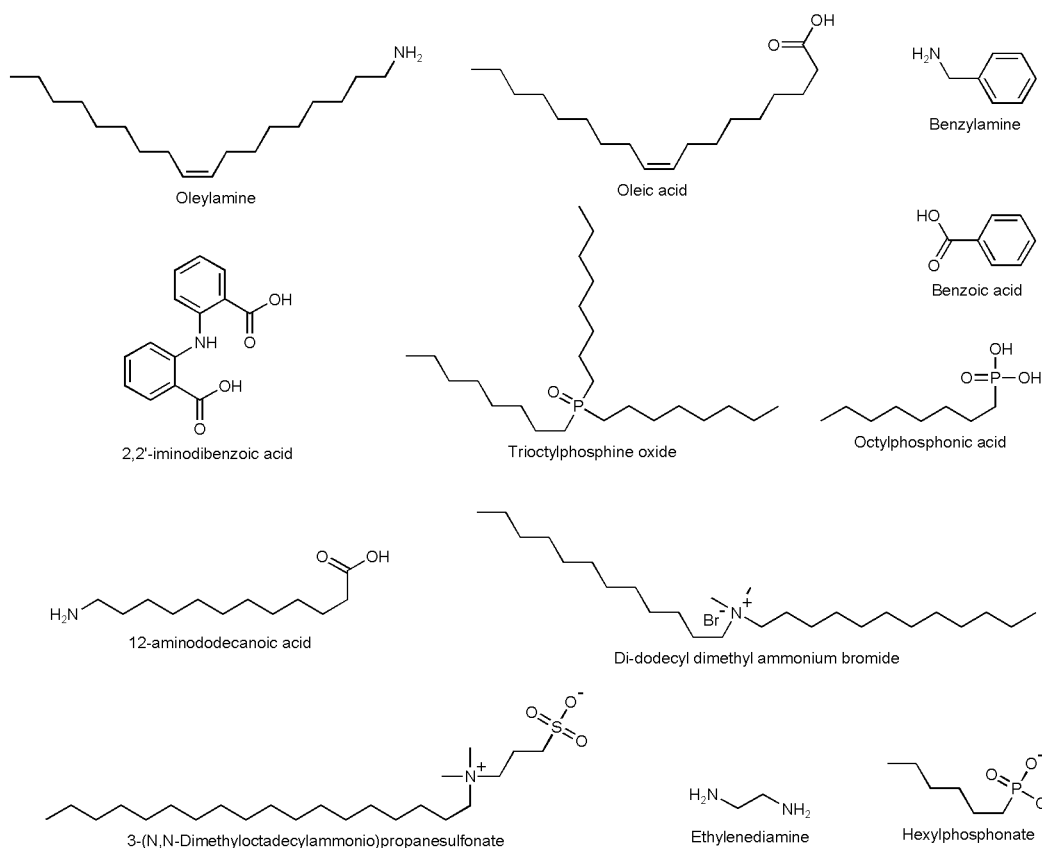**Figure 3.** A brief summary of the ligands applied for surface passivation of perovskite NCs.

Doping is widely applied to tune the emission peaks of perovskite NCs because of energy transfer from the charge carriers of hosts to dopants (i.e., for Mn-doped $CsPbCl_3$, excitation energy is transferred to a Mn d-state, resulting in yellow-orange d-d emission).[49-55] Both iso-valent (divalent) and heterovalent (monovalent and trivalent) metal ions have been reported for doping of perovskite NCs.[55, 56-60] In addition to tuning the emission peak, doping is also an effective strategy for reducing defects in perovskite NCs without influencing their size or crystal structure. Here, we focus only on cases related to the defect chemistry relevant to metal or rare-earth doping. Doping can be realized either by growth doping, in which metal ions are directly introduced into the precursor, or by diffusion doping, in which added dopant ions substitute for host ions, usually via post-treatment because of fast ion exchange with perovskite NCs.[51] The doped metal ions are distributed either in the lattice, which could induce changes in the lattice constant, or on the surfaces of NCs. Numerous studies have reported positive roles of metal-ion or rare-earth doping in suppressing crystallographic defects, including point defects (vacancies) or structure disorder (distortion of the $[PbX_6]$ octahedra), in perovskite NCs.

Even with fine optimization of synthetic factors such as reaction temperature and duration, precursors, and reactant stoichiometry, the imperfect assembly of constituents during a reaction still exists and is the main reason for low PLQY in violet-emitting $CsPbX_3$ NCs. These imperfections in crystals, likely due to vacancies and/or surface excess Pb and/or distorted $[PbX_6]$ octahedra, could deteriorate the short-range order of the lattice and act as trapping centers for photogenerated carriers, thus resulting in poor PLQYs for band-edge emission. Yong et al. reported that incorporating a small amount of divalent foreign ions, Ni^{2+} in their case, into the $CsPbX_3$ matrix could substantially increase the defect formation energy and thus enhance the

short-range order of the lattice without introducing new recombination channels. Ni doping caused substantially enhanced band-edge emission of $CsPbCl_3$ NCs, and the nonradiative recombination rate decreased from 378.29 μs^{-1} in undoped NCs to 1.90 μs^{-1} in Ni-11.9%, confirming the suppression of nonradiative recombination enabled by Ni doping. (Figure 4a-4b). The incorporation of Ni^{2+} ions into $CsPbCl_3$ NCs led to strong single-color violet emission with a maximum PLQY of 96.5%. The Cl vacancy possessed an in-gap state for undoped $CsPbCl_3$ without changing the band gap relative to that of doped-$CsPbCl_3$ without any defect (Figure 4c-4d). Density functional theory (DFT) calculations revealed that doping increased the defect formation energy of V_{Cl}, V_{Cs}, and V_{Pb} with respect to that of undoped NCs.[61]
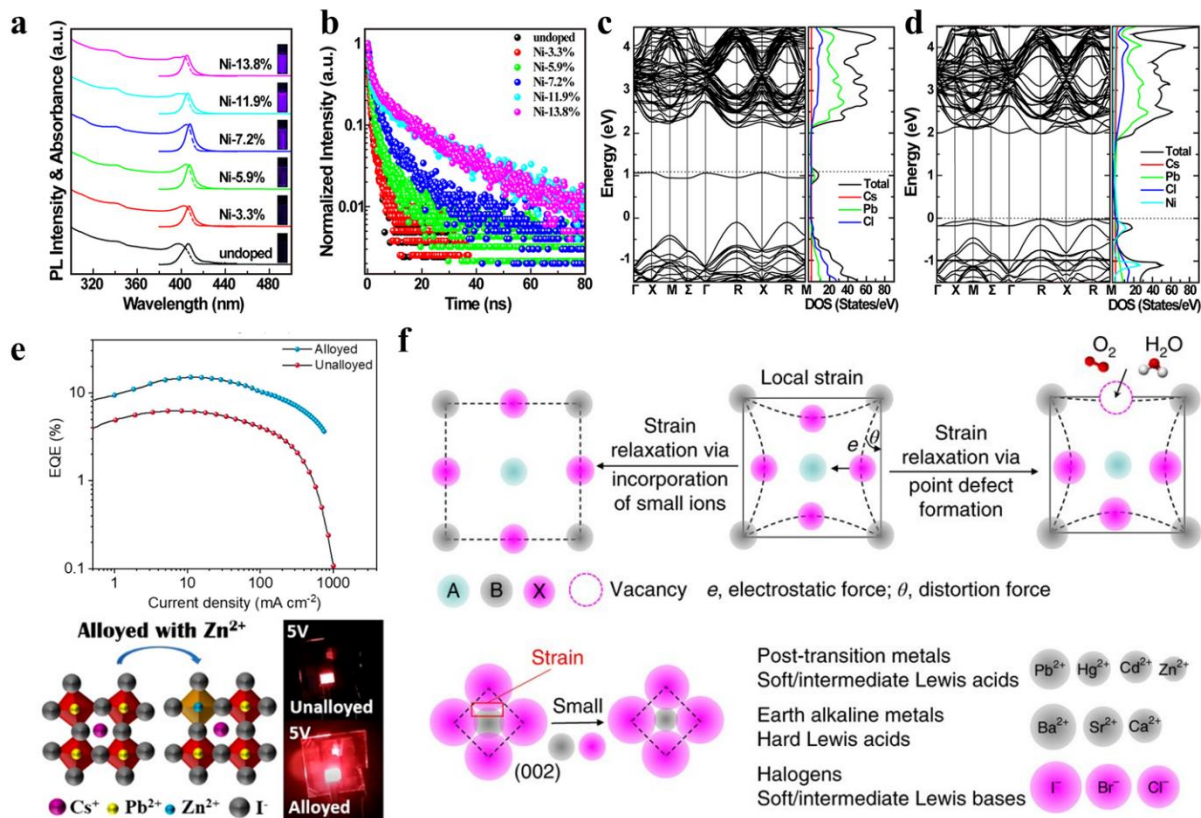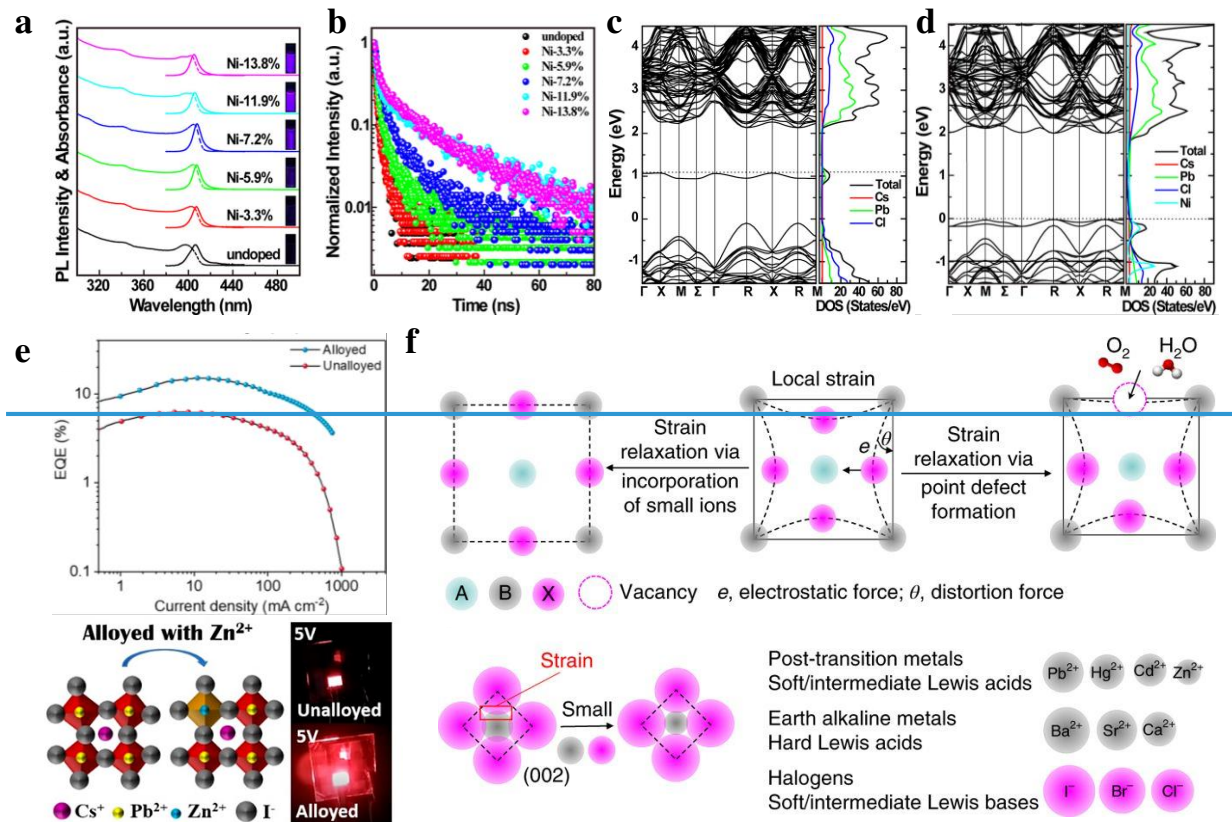
Figure 4. a. Absorption and PL spectra of undoped and doped CsPbCl$_3$ NCs. **b.** PL decay traces of undoped and doped CsPbCl$_3$ NCs. **c.** and **d.** Band structure and density of states (DOS) of undoped CsPbCl$_3$ with a Cl vacancy and Ni-doped CsPbCl$_3$ without any defect, respectively. Adapted from ref 61. Copyright 2018 American Chemical Society. **e.** EQEs for CsPbI$_3$ and alloyed CsPb$_{0.64}$Zn$_{0.36}$I$_3$ NCs LEDs, and photographs of the respective working LEDs. Adapted from ref 64. Copyright 2019 American Chemical Society. **f.** Schematic illustrating the local strain, which is reduced either by the formation of point defects or by the incorporation of small ions. Adapted from ref 36. Copyright 2018 Nature Publishing Group.

Bi et al. reported doping smaller Cu^{2+} ions into CsPb(Br/Cl)$_3$. The results showed that the Cu^{2+} doping induced a lattice contraction and eliminated halide vacancies, which increased the lattice formation energy and improved the short-range order of the doped perovskite NCs. It was

16

found that both the thermal stability and the optical performance of NCs were improved upon doping with Cu^{2+}.[62]

The divalent metal ion Zn^{2+} was also proven effective for defect passivation both in $CsPbBr_3$ and $CsPbI_3$ NCs. The PLQY of $ZnBr_2$-doped $CsPbBr_3$ NCs (PLQY = 78%) was markedly higher than that of pristine-$CsPbBr_3$ NCs (PLQY = 54%) without a shift in the emission peak. Two possible mechanisms were proposed to explain the defect passivation effect induced by Zn^{2+} doping: (1) a lead bromide adlayer can be formed on the surface of $CsPbBr_3$ NCs due to the favorable formation energetics attained when $ZnBr_2$ is introduced into reaction solutions; (2) the presence of $ZnBr_2$ during synthesis possibly leads to lead bromide-rich surface termination by significantly altering growth conditions. Both proposed surface structures indicate inorganically passivated and highly stable surfaces of $ZnBr_2$-$CsPbBr_3$ NCs. Several other metal bromides, such as $InBr_3$ and $CuBr_2$, have also proved to be effective.[63]

Defect passivation enabled by alloying Zn^{2+} into $CsPbI_3$ NCs has also been demonstrated. The defect density of $CsPbI_3$ and $CsPb_{0.64}Zn_{0.36}I_3$ NC films extracted by the space-charge-limited current (SCLC) method were estimated to be 1.26×10^{17} and 1.75×10^{16} cm^{-3}, respectively, representing a substantial decrease of almost an order of magnitude upon the incorporation of Zn^{2+}. The atomic ratio of I to (Zn plus Pb) was increased, and the surface elemental environment changed from a lead-rich state to an iodine-rich state after introducing Zn^{2+}. Moreover, the alloying also improved the stability by lattice contraction, and the α-phase of the NCs could remain stable in air for 70 days. Regarding device performance, the best-performing LED achieved a high luminance of 2202 cd m^{-2}, representing a 4-fold increase versus that of the Zn-free material; a low turn-on voltage of 2.0 V; and a peak EQE of 15.1% (Figure 4e).[64]

Navendu et al. reported doping of Cd^{2+} into $CsPbCl_3$ NCs by $CdCl_2$ post-treatment. The PLQY of $CsPbCl_3$ NCs (PL peak ~ 406 nm) was increased to near unity (96 ± 2%) with the $CdCl_2$ post-treatment. Time-resolved photoluminescence lifetime (TRPL) and ultrafast transient absorption (TAS) measurements confirmed the removal of nonradiative defect states of the $CsPbCl_3$ NCs after the $CdCl_2$ post-treatment.[65]

Digging deeper, an excellent example illustrating the mechanism of small iso-valent metal-ion (Zn^{2+}, Cd^{2+}, etc.) doping is the reduction of the defect population of a $(Cs,FA,MA)Pb(I_{0.85}Br_{0.15})_3$ polycrystalline thin film by such doping (Figure 4f). Strain originates from the ionic size mismatch between the A cation and the lead-halide cage size, resulting in cage distortions and BX_6 octahedron tilting in the ABX_3 perovskite structure. To release the strain in $FAPbI_3$, point defect formation is favorable, and this mechanism of lattice relaxation via vacancy formation is well known in oxide perovskites. The incorporation of small iso-valent metal ions prevents the formation of defects by opening a new lattice strain relaxation pathway, alternative to vacancy formation in perovskites for lattice strain relaxation. Saidaminov et al. used Cd^{2+}, which is iso-valent to Pb^{2+} but has a smaller ionic radius, for further relaxation of lattice strain without introducing traps. DFT calculations showed that Cd incorporation indeed relaxes the lattice strain and suppresses the formation energy of I vacancy by ≥ 0.5 eV.[36]

Defects in crystalline semiconductors can be categorized either as interruptions of an otherwise perfect crystal lattice (crystallographic defects) or as foreign atoms in the lattice (impurities).[64] Based on the definitions of the defects, heterovalent dopants as foreign atoms could create impurity levels, either deep or shallow traps, in the band gap of the host semiconductor.[67-68] However, this approach could be beneficial for promoting light emission when the doping of heterovalent metal ions only induces shallow states near the band edge of the conduction band

(CB) of perovskite NCs. Doping with heterovalent Ce^{3+} ions has been reported to not introduce trap states because of the similar ionic radii of Ce^{3+} and Pb^{2+} and because of the formation of a higher conduction band energy level with bromine relative to that formed with the Pb^{2+} cation.[69] When doping 2.88% Ce^{3+} (atomic ratio of Ce relative to Pb) into $CsPbBr_3$ NCs, the PLQY of $CsPbBr_3$ NCs reached up to 89%, compared with 41% for undoped NCs. TAS results showed that Ce^{3+} doping induced an increase in the density of the near-band-edge state. Filling of the CB with extra electrons donated by dopants would normally result in greater band-edge PL emission when the influence of nonradiative trap states on this PL channel is insignificant; otherwise, PL quenching would occur. The near-band-edge states induced by Ce^{3+} doping are radiative in nature and thus provide more emissive channels than nonradiative trapping channels.

Recently, Jun et al. further uncovered the mechanism of heterovalent doping in $CsPbBr_3$ by calculating the dopant defect formation energies and charge-transition levels using high-level DFT.[70] The results show that Bi^{3+} dopants introduce deep trap states (antisite Bi_{Pb} and interstitial Bi_i) that are responsible for PL quenching. However, the Ce^{3+} dopants enhance the $CsPbBr_3$ lattice order and enrich the conduction band-edge states through antisite Ce_{Pb}, causing PL enhancement.

Vacancies are abundant on the surface of perovskite NCs. Unlike the doping strategy, which mainly aims to reduce structure ($[PbX_6]$ octahedra) disorder and increase the defect formation energy, the elemental compensation strategy aims to annihilate surface vacancies by donating the elements required to fill these vacancy sites. Metal halides could provide both metal ions and halides for the surface elemental compensation of perovskite NCs. The post-treatment strategy involving the direct addition of $PbBr_2$ to a pristine solution of $CsPbBr_3$ NCs induces stronger ligand binding at the NC surface and introduces excess Br^-, both of which benefit the PL efficiency.[71] Halogen defects are abundant on the surface of $CsPbX_3$ QDs, and a facile method was applied to

simultaneously enhance the stability and PLQYs of $CsPbX_3$ QDs by a ZnX_2/hexane solution post-treatment. After the post-treatment, halogen vacancies were completely removed, as verified by high-resolution transmission electron microscopy (HRTEM), resulting in enhanced stability and PL (Figure 5a and 5b). The ZnX_2/hexane solution post-treatment is universal to several compositions, including $CsPbCl_3$, $CsPbBr_3$, and $CsPbI_3$.[72]

The small monovalent cation potassium (K^+) has proven to be a highly effective passivator in polycrystalline perovskite films. Although it cannot be incorporated into the perovskite lattice, K^+ is effective in passivating the surface of perovskite grains. Abdi-Jalebi et al. used potassium iodide to introduce excess iodide into perovskite precursor solutions and thereby compensate for any halide vacancies. The external photoluminescence quantum efficiency (PLQE) of the authors' $(Cs,FA,MA)Pb(I_{0.85}Br_{0.15})_3$ perovskite films reached a very high PLQE of 66% when the fraction of potassium ions relative to the total number of monovalent cations in the precursor solution was 0.40 (Figure 5c).[73] As illustrated in Figure 5d, the excess halides fill these vacancies, thereby passivating the nonradiative recombination pathways and leading to high luminescence efficiencies. The excess halides are immobilized in the form of benign, potassium-rich, halide-sequestering species at the grain boundaries and surfaces, thereby inhibiting halide migration and suppressing any additional nonradiative decay arising from interstitial halides. However, K^+ passivation has not yet been demonstrated in NCs.

Similarly to the passivation mechanism of K^+, trivalent metal chloride salts, i.e., YCl_3, can fill vacancies on the surface of NCs and were therefore used for the dual-surface passivation of $CsPbCl_3$ NCs. A Cl-rich surface and constant Pb 4f core-level peak were observed by X-ray photoelectron spectroscopy, which indicated that Y^{3+} only anchored to the surface, bonded to uncoordinated Pb atoms, and subsequently suppressed the formation of surface nonradiative

recombination centers. However, when Y-acetate salt was chosen as an additive to replace YCl_3, the enhancement in the PLQY was not as outstanding as that achieved by YCl_3, revealing Cl^- passivation in addition to the positive role played by Y^{3+} (Figure 5e and 5f). DFT results indicate that Y^{3+} and Cl^- ions efficiently occupy surface Pb-Cl ion vacancies, enriching the density of states in the conduction band without creating any mid-gap states. This dual-passivation strategy resulted in a remarkable increase in the PLQY, from 1 to 60%, while maintaining the shape, size, and crystal structure.[74]

The Cl^- anions carried by $SrCl_2$ are also able to efficiently passivate surface defect states of $CsPbI_3$ NCs, thus converting nonradiative trap states to radiative states. Surface Cl^- ion passivation was shown to enhance the PLQY (by up to 84%) of $CsPbI_3$ NCs, which were employed to produce LEDs with a high external quantum yield of 13.5%.[75]

The thiocyanate (SCN^-) anion can be incorporated into the perovskite lattice. Partial replacement of halides with the SCN^- ion to form mixed-anion perovskites has been shown to benefit structure stability against moisture.[76-78] Moreover, a $CH_3NH_3Pb(SCN)_xI_{3-x}$ polycrystalline thin film was reported to exhibit large crystal sizes with decreased trap states.[79-81] The SCN^- ion also plays positive roles in suppressing defects in perovskite NCs. Koscher et al. demonstrated a surface treatment involving SCN^- that improved the PLQY of $CsPbBr_3$ to near unity (Figure 5g). Salt powders, either ammonium (NH_4SCN) or sodium thiocyanate ($NaSCN$), were directly introduced into the solution for SCN^- treatment. The chemical effect of the treatment indicated that no more than 10~15% of the surface ligands were replaced with thiocyanate, but the composition of the NC surface changed from ~10% lead-rich to a stoichiometric 1:3 ratio of Pb to Br. This treatment is an effective way to remove excess Pb from the surface, consequently removing trap

states induced by excess lead on the surface of NCs and making the NCs into near-unity green emitters.[82]

Blue-emitting perovskite NCs have lower PLQYs than green- and red-emitting NCs because of easily formed defects and insufficient surface passivation.[83-84] An in situ $PbBr_6^{4-}$ octahedron passivation strategy involving excess Br^- passivation to achieve 96% absolute QY blue emission from $CsPbBr_3$ nanoplatelets (NPLs) was reported.[85] To construct intact $PbBr_6^{4-}$ octahedra, additional Br^- was introduced by adding HBr aqueous solution into the synthesis system to drive the ionic equilibrium to form intact Pb-Br octahedra (Figure 5h). The reduced number of Br vacancies and suppressed nonradiative recombination processes were well indicated by a reduced Urbach energy and a longer transient absorption delay. Blue LEDs using NPLs were fabricated, and a high EQE of 0.124% was achieved. Cl passivation induced by metal chlorides and ammonium chloride salts was applied to boost the PLQY of blue-emitting $CsPbCl_3$ NCs.[84] Cl passivation was also used to boost the PLQY of lead-free $MA_3Bi_2Br_9$ QDs to 54.1% at a wavelength of 422 nm, a new PLQY record for blue-emitting, lead-free perovskite NCs. Because of the incompatible crystal structures between $MA_3Bi_2Br_9$ and $MA_3Bi_2Cl_9$ and the careful kinetic control achieved during synthesis, Cl^- anions are engineered to localize mainly on the surface of NCs and act as passivating ligands, effectively suppressing surface defects and enhancing the PLQY.[83]
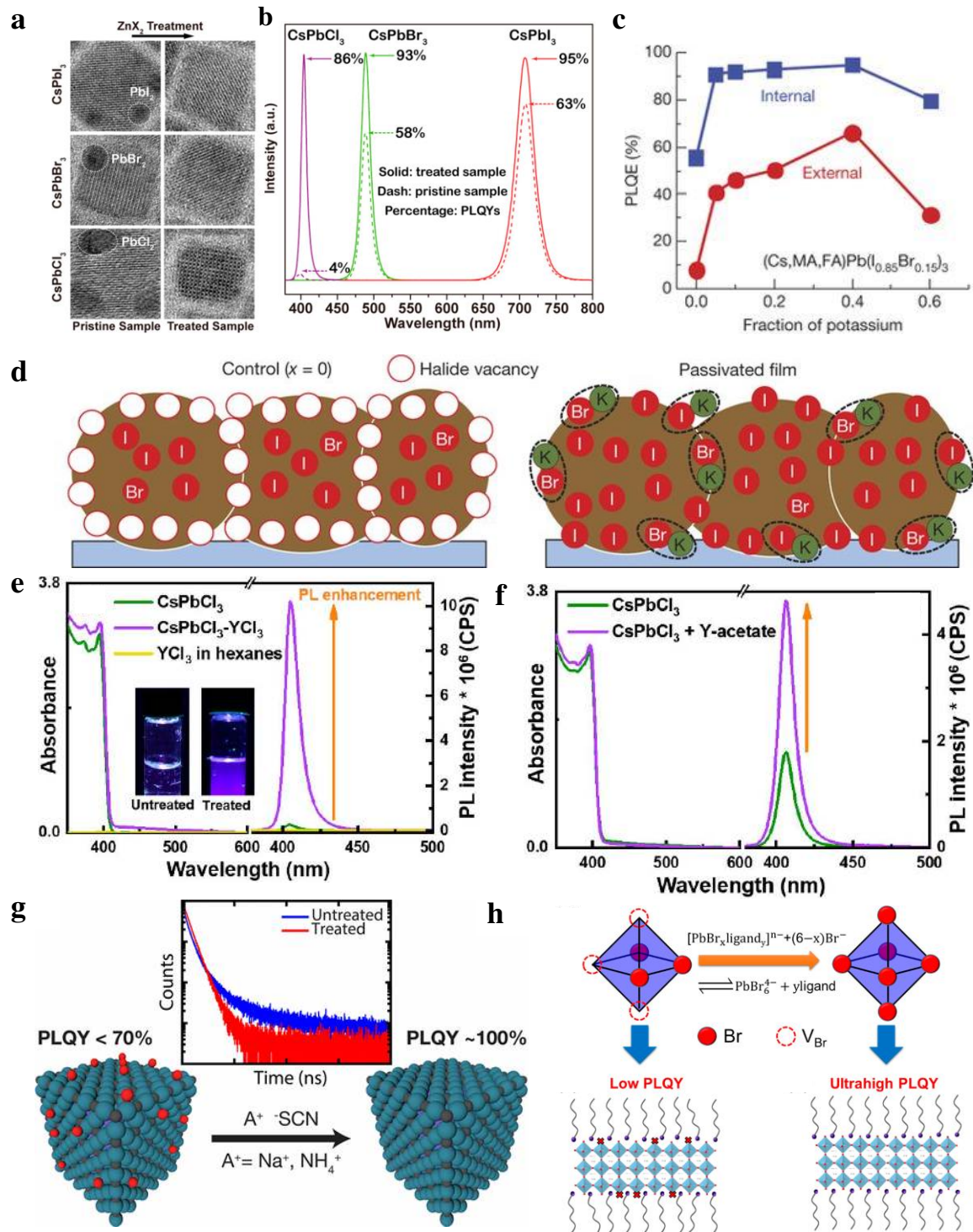
Figure 5. a. HRTEM images of pristine CsPbCl₃, CsPbBr₃, and CsPbI₃ NCs and ZnX₂-treated CsPbCl₃, CsPbBr₃, and CsPbI₃ NCs. The removal of the "black dots" on the NCs after treatment can be clearly observed. **b.** Photoluminescence spectra of pristine and ZnX₂-treated CsPbX₃ NCs.

Adapted from ref 72. Copyright 2019 American Chemical Society. **c.** External photoluminescence quantum efficiency (PLQE) of passivated perovskite thin films with increasing fraction of potassium, x. **d.** Schematic of a cross-section of a film showing halide-vacancy management in cases of excess halide, in which the surplus halide is immobilized through complexing with potassium into benign compounds at the grain boundaries and surfaces. Adapted from ref 73. Copyright 2018 Nature Publishing Group. **e.** Steady-state optical absorption and PL spectra for the as-synthesized $CsPbCl_3$ NCs dispersed in hexanes before and after YCl_3 surface passivation; insets are photographs of the untreated and YCl_3-treated NCs under 365-nm UV illumination. **f.** Steady-state absorption and relative PL spectrum for both pristine and yttrium acetate-treated NCs. Adapted from ref 74. Copyright 2018 American Chemical Society. **g.** Time-resolved photoluminescence lifetimes (TRPLs) of aged $CsPbBr_3$ before and after ammonium thiocyanate treatment and schematic of the interaction between thiocyanate and $CsPbBr_3$ NC surface defect sites. Adapted from ref 82. Copyright 2017 American Chemical Society. **h.** Schematic demonstration of $PbBr_6^{4-}$ octahedra with and without V_{Br}. By introducing a HBr complex solution, the ionic equilibrium was driven to the intact-octahedra side. Adapted from ref 85. Copyright 2018 American Chemical Society.

In a core-shell NC, the shell provides a physical barrier between the optically active core and the surrounding medium, reducing the sensitivity of the optical properties of the core to changes in the local environment of the NC's surface in the presence of oxygen or water molecules. Moreover, the shell provides efficient passivation of surface trap states, resulting in a strongly enhanced PLQY.[86] Therefore, construction of a core-shell structure is highly attractive for improving both the PLQY and stability of perovskite NCs.

The most efficient green perovskite LED reported to date, with a quantum efficiency of over 20%, is based on a $CsPbBr_3$/MABr quasi-core-shell structure, which represents a good example that can be transferred to NCs (Figure 6a-6b).[10] The $CsPbBr_3$/MABr quasi-core-shell was constructed by mixing a pre-synthesized $CsPbBr_3$ perovskite with a MABr additive. A shell of MABr is formed between the grain boundaries of $CsPbBr_3$, and another layer of MABr caps the $CsPbBr_3$, forming the quasi-core-shell structure. Results showed that the MABr shell reduced the number of defects in $CsPbBr_3$/MABr perovskite films by a factor of four compared with the number observed in a single-layer $CsPbBr_3$ film. Moreover, the $CsPbBr_3$/MABr films possessed a 50% longer radiative lifetime than did pure $CsPbBr_3$, which was attributed to the decrease in the concentration of defects.

NC/silica composites were also synthesized and showed high PLQY and extremely high stability in air (Figure 6c). (3-Aminopropyl)triethoxysilane (APTES) could undergo hydrolysis induced by trace water vapor in air, and a silica matrix subsequently formed slowly on perovskite NCs. The amino group in APTES could effectively passivate the NC surface to maintain the original high PLQY.[87]

Surface passivation by an isocrystalline core-shell structure could internalize surface-bound dopant ions and enhance the relative intensity of dopant emission. A Mn^{2+}-doped $CsPbCl_3$ NC/undoped $CsPbCl_3$ core-shell structure was adopted to protect the surface dopant ions (Mn^{2+}) and enhance the dopant light emission (Figure 6d).[88] To grow a $CsPbCl_3$-shell layer, the Mn^{2+}-doped $CsPbCl_3$ NCs were re-dispersed in toluene, followed by the addition of a specific volume of a solution consisting of Pb^{2+} and Cs^+ precursors for overgrowth with a $CsPbCl_3$ shell under vigorous stirring. It is well known that luminescent ions close to the surface experience faster decay as a result of energy transfer to surface defects. By applying an undoped $CsPbCl_3$ shell, the

lifetime of Mn^{2+} emission can be appreciably prolonged, as confirmed by a reduced quenching effect from surface defect sites.
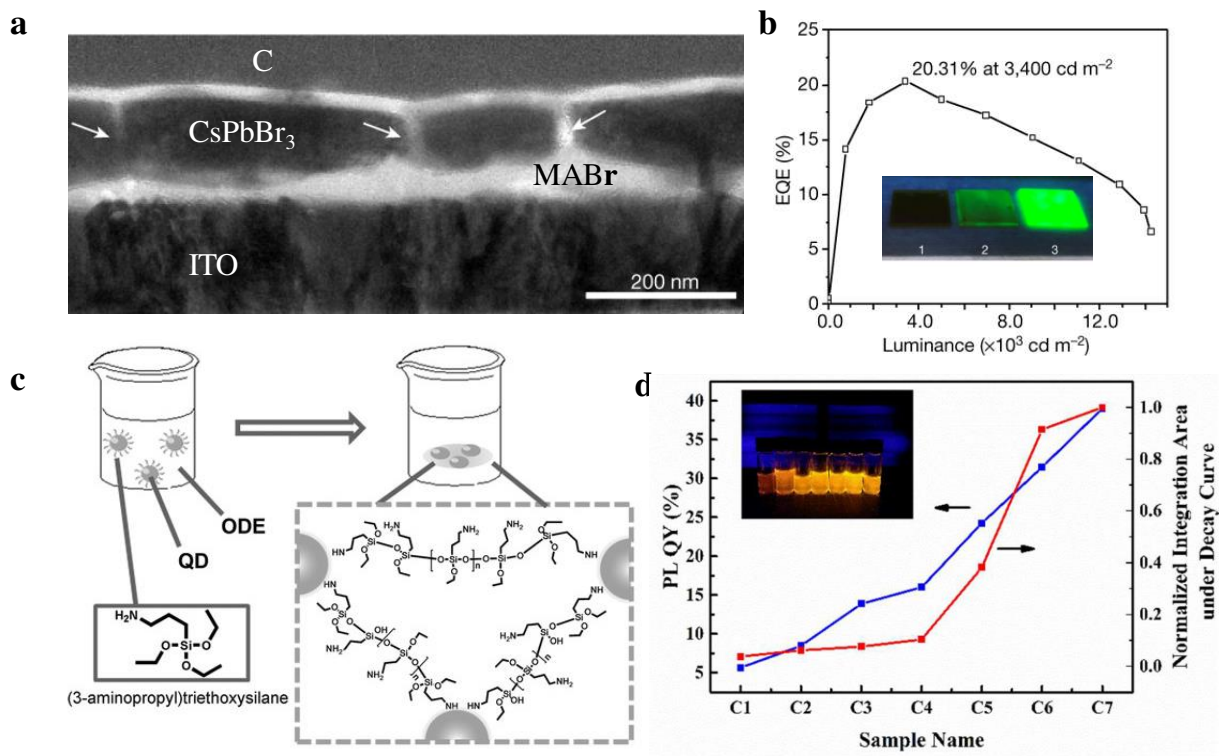

Figure 6. a. Cross-sectional TEM image of a quasi-core-shell $CsPbBr_3$/MABr structure. White arrows indicate the MABr shell (the grain boundary). **b.** EQE characteristics of the best-performing quasi-core-shell $CsPbBr_3$/MABr LEDs. Inset: photographs of single-layer $CsPbBr_3$, bilayer $CsPbBr_3$/MABr, and quasi-core-shell $CsPbBr_3$/MABr perovskite films under UV light. Adapted from ref 10. Copyright 2018 Nature Publishing Group. **c.** Schematic illustration of formation of QD/silica composites. Adapted from ref 87. Copyright 2016 Wiley‐VCH. **d.** Effect of isocrystalline core-shell (ICS) growth on the relative PLQY and integrated area under the Mn^{2+} luminescence decay curves for Mn^{2+}-doped $CsPbCl_3$ NCs. Blue line: evolution of PLQY as a function of shell thickness. Samples C1 to C7 are Mn^{2+}:$CsPbCl_3$ without a $CsPbCl_3$ shell to

Mn^{2+}:CsPbCl$_3$ with the thickest CsPbCl$_3$ shell from left to right. Adapted from ref 88. Copyright 2017 American Chemical Society.

Despite the remarkable success and progress achieved, many challenges remain to be addressed concerning passivation strategies and the understanding of defect chemistry for further improving perovskite NC light-emitting devices. We conclude by listing several crucial challenges for further research.

(1) Ligand detachment and self-assembly. The ligands of NCs suspended in solution are in a dynamic equilibrium between the crystal NC's surface and the solution. Over time, ligands can detach from the surface of the NCs and scavenge lead or halide ions on the surface of QDs, which creates more vacancies. After ligand detachment, the NCs are easily aggregated and regrow due to the reduced barrier from the surface ligands and easily moving ions of perovskite NCs.

(2) Defect species in NCs and full passivation of different types of defects. The types of defects that actually exist in NCs of various composition and the corresponding population should be revealed for target passivation.

(3) Composition-dependent defect chemistry. Changing composition can dramatically vary the defect chemistry of perovskite NCs and represents one of the main reasons for the inferior performance of blue-emitting perovskites compared with the performance of green- and red-emitting perovskites. For blue-emitting mixed-halide perovskites (CsPbBr$_x$Cl$_{3-x}$), Cl vacancies (V_{Cl}) are deep traps and highly energetically favorable. An effective defect passivation strategy for blue-emitting mixed-halide perovskites remains to be established.

(4) Insightful understanding of passivation mechanism. A series of strategies have been proposed to realize high-efficiency PL from halide perovskite NCs. However, in many cases the detailed

investigations of NC's structures remain missing. Systematic structural and photophysical characterizations coupled with first-principles calculations could deepen the understanding of underlying mechanisms for the passivation methods used. For instance, doping engineering can be used for optimization of the performance of perovskite NCs, but the critical factors governing the doping efficiency and the exact distribution of dopants in NCs remain elusive in most doped NCs.[89] Similarly, for post-synthetic treatment, it requires a deeper understanding of the role of metal cations that play in the removal of defects.

(5) Core-shell perovskite NCs. At present, construction of perovskite core-shell NCs remains a significant challenge. There are numerous perovskite compositions, the band gaps of which can be easily tuned. Thus, numerous perovskite-perovskite core-shell structures can be constructed, and new interfacial chemistry and physics could be further explored. Many successfully fabricated heterojunction core-shell structures, such as CdSe/CdS, CdSe/CdZnS, and InP/ZnS core-shell NCs, have been well studied. Other semiconductors with a small lattice mismatch with perovskites should be explored to passivate surface trap states and encapsulate the environmentally sensitive perovskite NCs inside.

In summary, tremendous progress has been made in eliminating defects in perovskite NCs for fabricating efficient light-emitting devices. This Perspective discusses the strategies established for defect reduction and examines the potential mechanisms that underlie these strategies. Many methods for reducing the defect states of NCs have been developed, including advanced NC syntheses, new surface-capping strategies, doping with metal ions and rare earths, engineering elemental compensation, and the translation of core-shell heterostructures. Nevertheless, various challenges await to be addressed, and further research efforts are needed to solve these problems.

Additional information

Correspondence and requests for materials should be addressed to E.H.S. (ted.sargent@utoronto.ca) and O.M.B. (osman.bakr@kaust.edu.sa).

Acknowledgement

Competing financial interests

The authors declare no competing financial interests.

Reference

1. Xiao, Z.; Kerner, R. A.; Zhao, L.; Tran, N. L.; Lee, K. M.; Koh, T.-W.; Scholes, G. D.; Rand, B. P. Efficient Perovskite Light-Emitting Diodes Featuring Nanometre-sized Crystallites. *Nat. Photonics* **2017,** *11*, 108.

2. Akkerman, Q. A.; Rainò, G.; Kovalenko, M. V.; Manna, L. Genesis, Challenges and Opportunities for Colloidal Lead Halide Perovskite Nanocrystals. *Nat. Mater.* **2018,** *17*, 394-405.

3. Chen, Q.; Wu, J.; Ou, X.; Huang, B.; Almutlaq, J.; Zhumekenov, A. A.; Guan, X.; Han, S.; Liang, L.; Yi, Z.*; et al.* All-Inorganic Perovskite Nanocrystal Scintillators. *Nature* **2018,** *561*, 88-93.

4. Zhang, L.; Yang, X.; Jiang, Q.; Wang, P.; Yin, Z.; Zhang, X.; Tan, H.; Yang, Y.; Wei, M.; Sutherland, B. R.*; et al.* Ultra-Bright and Highly Efficient Inorganic Based Perovskite Light-Emitting Diodes. *Nat. Commun.* **2017,** *8*, 15640.

5. Swarnkar, A.; Marshall, A. R.; Sanehira, E. M.; Chernomordik, B. D.; Moore, D. T.; Christians, J. A.; Chakrabarti, T.; Luther, J. M. Quantum Dot–Induced Phase Stabilization of α-CsPbI$_3$ Perovskite for High-Efficiency Photovoltaics. *Science* **2016,** *354*, 92-95.

6. Wang, N.; Cheng, L.; Ge, R.; Zhang, S.; Miao, Y.; Zou, W.; Yi, C.; Sun, Y.; Cao, Y.; Yang, R.*; et al.* Perovskite Light-Emitting Diodes Based on Solution-Processed Self-Organized Multiple Quantum Wells. *Nat. Photonics* **2016,** *10*, 699.

7. Song, J.; Li, J.; Li, X.; Xu, L.; Dong, Y.; Zeng, H. Quantum Dot Light-Emitting Diodes Based on Inorganic Perovskite Cesium Lead Halides (CsPbX$_3$). *Adv. Mater.* **2015,** *27*, 7162-7167.

8. Zhang, X.; Liu, H.; Wang, W.; Zhang, J.; Xu, B.; Karen, K. L.; Zheng, Y.; Liu, S.; Chen, S.; Wang, K.*; et al.* Hybrid Perovskite Light-Emitting Diodes Based on Perovskite Nanocrystals with Organic–Inorganic Mixed Cations. *Adv. Mater.* **2017,** *29*, 1606405.

9. Bodnarchuk, M. I.; Boehme, S. C.; ten Brinck, S.; Bernasconi, C.; Shynkarenko, Y.; Krieg, F.; Widmer, R.; Aeschlimann, B.; Günther, D.; Kovalenko, M. V. Rationalizing and Controlling the Surface Structure and Electronic Passivation of Cesium Lead Halide Nanocrystals. *ACS Energy Lett.* **2018,** *4*, 63-74.

10. Lin, K.; Xing, J.; Quan, L. N.; de Arquer, F. P. G.; Gong, X.; Lu, J.; Xie, L.; Zhao, W.; Zhang, D.; Yan, C.*; et al.* Perovskite Light-Emitting Diodes with External Quantum Efficiency Exceeding 20 Per Cent. *Nature* **2018,** *562*, 245-248.

11. Chiba, T.; Hayashi, Y.; Ebe, H.; Hoshi, K.; Sato, J.; Sato, S.; Pu, Y.-J.; Ohisa, S.; Kido, J. Anion-Exchange Red Perovskite Quantum Dots with Ammonium Iodine Salts for Highly Efficient Light-Emitting Devices. *Nat. Photonics* **2018,** *12*, 681-687.

12. Cao, Y.; Wang, N.; Tian, H.; Guo, J.; Wei, Y.; Chen, H.; Miao, Y.; Zou, W.; Pan, K.; He, Y.*; et al.* Perovskite Light-Emitting Diodes Based on Spontaneously Formed Submicrometre-Scale Structures. *Nature* **2018,** *562*, 249-253.

13. Zhang, Y.; Sun, R.; Ou, X.; Fu, K.; Chen, Q.; Ding, Y.; Xu, L.-J.; Liu, L.; Han, Y.; Malko, A. V.*; et al.* Metal Halide Perovskite Nanosheet for X-ray High-Resolution Scintillation Imaging Screens. *ACS Nano* **2019,** *13*, 2520-2525.

14. Huang, H.; Polavarapu, L.; Sichert, J. A.; Susha, A. S.; Urban, A. S.; Rogach, A. L. Colloidal Lead Halide Perovskite Nanocrystals: Synthesis, Optical Properties and Applications. *NPG Asia Mater.* **2016,** *8*, e328.

15. Yuan, M.; Quan, L. N.; Comin, R.; Walters, G.; Sabatini, R.; Voznyy, O.; Hoogland, S.; Zhao, Y.; Beauregard, E. M.; Kanjanaboos, P.*; et al.* Perovskite Energy Funnels for Efficient Light-Emitting Diodes. *Nat. Nanotechnol.* **2016,** *11*, 872.

16. Chen, Z.; Zhang, C.; Jiang, X.-F.; Liu, M.; Xia, R.; Shi, T.; Chen, D.; Xue, Q.; Zhao, Y.-J.; Su, S.*; et al.* High-Performance Color-Tunable Perovskite Light Emitting Devices through Structural Modulation from Bulk to Layered Film. *Adv. Mater.* **2017,** *29*, 1603157.

17. Bade, S. G. R.; Li, J.; Shan, X.; Ling, Y.; Tian, Y.; Dilbeck, T.; Besara, T.; Geske, T.; Gao, H.; Ma, B.*; et al.* Fully Printed Halide Perovskite Light-Emitting Diodes with Silver Nanowire Electrodes. *ACS Nano* **2016,** *10*, 1795-1801.

18. Dong, Y.; Zhao, Y.; Zhang, S.; Dai, Y.; Liu, L.; Li, Y.; Chen, Q. Recent Advances toward Practical Use of Halide Perovskite Nanocrystals. *J. Mater. Chem. A* **2018,** *6*, 21729-21746.

19. Wang, N.; Liu, W.; Zhang, Q. Perovskite-Based Nanocrystals: Synthesis and Applications beyond Solar Cells. *Small Methods* **2018,** *2*, 1700380.

20. Tanaka, K.; Kondo, T. Bandgap and Exciton Binding Energies in Lead-Iodide-Based Natural Quantum-Well Crystals. *Sci. Technol. Adv. Mater.* **2003,** *4*, 599-604.

21. Huang, J.; Yuan, Y.; Shao, Y.; Yan, Y. Understanding the Physical Properties of Hybrid Perovskites for Photovoltaic Applications. *Nat. Rev. Mater.* **2017,** *2*, 17042.

22. Park, Y.-S.; Guo, S.; Makarov, N. S.; Klimov, V. I. Room Temperature Single-Photon Emission from Individual Perovskite Quantum Dots. *ACS Nano* **2015,** *9*, 10386-10393.

23. Kim, Y.-H.; Wolf, C.; Kim, Y.-T.; Cho, H.; Kwon, W.; Do, S.; Sadhanala, A.; Park, C. G.; Rhee, S.-W.; Im, S. H.*; et al.* Highly Efficient Light-Emitting Diodes of Colloidal Metal–Halide Perovskite Nanocrystals beyond Quantum Size. *ACS Nano* **2017,** *11*, 6586-6593.

24. Swarnkar, A.; Chulliyil, R.; Ravi, V. K.; Irfanullah, M.; Chowdhury, A.; Nag, A. Colloidal CsPbBr3 Perovskite Nanocrystals: Luminescence beyond Traditional Quantum Dots. *Angew. Chem., Int. Ed.* **2015,** *127*, 15644-15648.

25. Sichert, J. A.; Tong, Y.; Mutz, N.; Vollmer, M.; Fischer, S.; Milowska, K. Z.; García Cortadella, R.; Nickel, B.; Cardenas-Daw, C.; Stolarczyk, J. K.*; et al.* Quantum Size Effect in Organometal Halide Perovskite Nanoplatelets. *Nano Lett.* **2015,** *15*, 6521-6527.

26. Xiao, Z.; Zhao, L.; Tran, N. L.; Lin, Y. L.; Silver, S. H.; Kerner, R. A.; Yao, N.; Kahn, A.; Scholes, G. D.; Rand, B. P. Mixed-Halide Perovskites with Stabilized Bandgaps. *Nano Lett.* **2017,** *17*, 6863-6869.

27. Xing, G.; Wu, B.; Wu, X.; Li, M.; Du, B.; Wei, Q.; Guo, J.; Yeow, E. K. L.; Sum, T. C.; Huang, W. Transcending the Slow Bimolecular Recombination in Lead-Halide Perovskites for Electroluminescence. *Nat. Commun.* **2017,** *8*, 14558.

28. Li, G.; Rivarola, F. W. R.; Davis, N. J. L. K.; Bai, S.; Jellicoe, T. C.; de la Peña, F.; Hou, S.; Ducati, C.; Gao, F.; Friend, R. H.*; et al.* Highly Efficient Perovskite Nanocrystal Light-Emitting Diodes Enabled by a Universal Crosslinking Method. *Adv. Mater.* **2016,** *28*, 3528-3534.

29. Protesescu, L.; Yakunin, S.; Bodnarchuk, M. I.; Krieg, F.; Caputo, R.; Hendon, C. H.; Yang, R. X.; Walsh, A.; Kovalenko, M. V. Nanocrystals of Cesium Lead Halide Perovskites ($CsPbX_3$, X = Cl, Br, and I): Novel Optoelectronic Materials Showing Bright Emission with Wide Color Gamut. *Nano Lett.* **2015,** *15*, 3692-3696.

30. Dong, Y.; Qiao, T.; Kim, D.; Parobek, D.; Rossi, D.; Son, D. H. Precise Control of Quantum Confinement in Cesium Lead Halide Perovskite Quantum Dots via Thermodynamic Equilibrium. *Nano Lett.* **2018,** *18*, 3716-3722.

31. Dutta, A.; Behera, R. K.; Pal, P.; Baitalik, S.; Pradhan, N. Near-Unity Photoluminescence Quantum Efficiency for All $CsPbX_3$ (X = Cl, Br and I) Perovskite Nanocrystals: A Generic Synthesis Approach. *Angew. Chem., Int. Ed.* **2019,** (doi:10.1002/anie.201900374).

32. Dutta, A.; Behera, R. K.; Dutta, S. K.; Das Adhikari, S.; Pradhan, N. Annealing $CsPbX_3$ (X= Cl and Br) Perovskite Nanocrystals at High Reaction Temperatures: Phase Change and Its Prevention. *J. Phys. Chem. Lett.* **2018,** *9*, 6599-6604.

33. Das Adhikari, S.; Behera, R. K.; Bera, S.; Pradhan, N. Presence of Metal Chloride for Minimizing the Halide Deficiency and Maximizing the Doping Efficiency in Mn(II)-Doped $CsPbCl_3$ Nanocrystals. *J. Phys. Chem. Lett.* **2019**, *10*, 1530-1536.

34. Tong, Y.; Bladt, E.; Aygüler, M. F.; Manzi, A.; Milowska, K. Z.; Hintermayr, V. A.; Docampo, P.; Bals, S.; Urban, A. S.; Polavarapu, L.*; et al.* Highly Luminescent Cesium Lead Halide Perovskite Nanocrystals with Tunable Composition and Thickness by Ultrasonication. *Angew. Chem., Int. Ed.* **2016,** *55*, 13887-13892.

35. Leng, M.; Yang, Y.; Chen, Z.; Gao, W.; Zhang, J.; Niu, G.; Li, D.; Song, H.; Zhang, J.; Jin, S. Surface Passivation of Bismuth-Based Perovskite Variant Quantum Dots to Achieve Efficient Blue Emission. *Nano Lett.* **2018,** *18*, 6076-6083.

36. Saidaminov, M. I.; Kim, J.; Jain, A.; Quintero-Bermudez, R.; Tan, H.; Long, G.; Tan, F.; Johnston, A.; Zhao, Y.; Voznyy, O.*; et al.* Suppression of Atomic Vacancies via Incorporation of Isovalent Small Ions to Increase the Stability of Halide Perovskite Solar Cells in Ambient Air. *Nat. Energy* **2018,** *3*, 648-654.

37. Liu, P.; Chen, W.; Wang, W.; Xu, B.; Wu, D.; Hao, J.; Cao, W.; Fang, F.; Li, Y.; Zeng, Y.*; et al.* Halide-Rich Synthesized Cesium Lead Bromide Perovskite Nanocrystals for Light-Emitting Diodes with Improved Performance. *Chem. Mater.* **2017,** *29*, 5168-5173.

38. Pan, J.; Shang, Y.; Yin, J.; De Bastiani, M.; Peng, W.; Dursun, I.; Sinatra, L.; El-Zohry, A. M.; Hedhili, M. N.; Emwas, A.-H. Bidentate Ligand-Passivated CsPbI$_3$ Perovskite Nanocrystals for Stable Near-Unity Photoluminescence Quantum Yield and Efficient Red Light-Emitting Diodes. *J. Am. Chem. Soc.* **2017,** *140*, 562-565.

39. Liu, F.; Zhang, Y.; Ding, C.; Kobayashi, S.; Izuishi, T.; Nakazawa, N.; Toyoda, T.; Ohta, T.; Hayase, S.; Minemoto, T. Highly Luminescent Phase-Stable CsPbI$_3$ Perovskite Quantum Dots Achieving Near 100% Absolute Photoluminescence Quantum Yield. *ACS Nano* **2017,** *11*, 10373-10383.

40. Tan, Y.; Zou, Y.; Wu, L.; Huang, Q.; Yang, D.; Chen, M.; Ban, M.; Wu, C.; Wu, T.; Bai, S. Highly Luminescent and Stable Perovskite Nanocrystals with Octylphosphonic Acid as a Ligand for Efficient Light-Emitting Diodes. *ACS Appl. Mater. Interfaces* **2018,** *10*, 3784-3792.

41. Luo, B.; Naghadeh, S. B.; Allen, A. L.; Li, X.; Zhang, J. Z. Peptide- Passivated Lead Halide Perovskite Nanocrystals Based on Synergistic Effect between Amino and Carboxylic Functional Groups. *Adv. Funct. Mater.* **2017,** *27*, 1604018.

42. Pan, J.; Quan, L. N.; Zhao, Y.; Peng, W.; Murali, B.; Sarmah, S. P.; Yuan, M.; Sinatra, L.; Alyami, N. M.; Liu, J. Highly Efficient Perovskite- Quantum- Dot Light- Emitting Diodes by Surface Engineering. *Adv. Mater.* **2016,** *28*, 8718-8725.

43. Pan, J.; Sarmah, S. P.; Murali, B.; Dursun, I.; Peng, W.; Parida, M. R.; Liu, J.; Sinatra, L.; Alyami, N.; Zhao, C.*; et al.* Air-Stable Surface-Passivated Perovskite Quantum Dots for Ultra-Robust, Single- and Two-Photon-Induced Amplified Spontaneous Emission. *J. Phys. Chem. Lett.* **2015,** *6*, 5027-5033.

44. Imran, M.; Ijaz, P.; Baranov, D.; Goldoni, L.; Petralanda, U.; Akkerman, Q.; Abdelhady, A. L.; Prato, M.; Bianchini, P.; Infante, I.*; et al.* Shape-Pure, Nearly Monodispersed $CsPbBr_3$ Nanocubes Prepared Using Secondary Aliphatic Amines. *Nano Lett.* **2018,** *18*, 7822-7831.

45. Vickers, E. T.; Graham, T. A.; Chowdhury, A. H.; Bahrami, B.; Dreskin, B. W.; Lindley, S.; Naghadeh, S. B.; Qiao, Q.; Zhang, J. Z. Improving Charge Carrier Delocalization in Perovskite Quantum Dots by Surface Passivation with Conductive Aromatic Ligands. *ACS Energy Lett.* **2018,** *3*, 2931-2939.

46. Krieg, F.; Ochsenbein, S. T.; Yakunin, S.; Ten Brinck, S.; Aellen, P.; Süess, A.; Clerc, B.; Guggisberg, D.; Nazarenko, O.; Shynkarenko, Y. Colloidal $CsPbX_3$ (X= Cl, Br, I) Nanocrystals 2.0: Zwitterionic Capping Ligands for Improved Durability and Stability. *ACS Energy Lett.* **2018,** *3*, 641-646.

47. Lee, S.; Park, J. H.; Lee, B. R.; Jung, E. D.; Yu, J. C.; Di Nuzzo, D.; Friend, R. H.; Song, M. H. Amine-Based Passivating Materials for Enhanced Optical Properties and Performance of Organic–Inorganic Perovskites in Light-Emitting Diodes. *J. Phys. Chem. Lett.* **2017,** *8*, 1784-1792.

48. Nenon, D. P.; Pressler, K.; Kang, J.; Koscher, B. A.; Olshansky, J. H.; Osowiecki, W. T.; Koc, M. A.; Wang, L.-W.; Alivisatos, A. P. Design Principles for Trap-Free $CsPbX_3$ Nanocrystals: Enumerating and Eliminating Surface Halide Vacancies with Softer Lewis Bases. *J. Am. Chem. Soc.* **2018**, *140*, 17760-17772.

49. Parobek, D.; Roman, B. J.; Dong, Y.; Jin, H.; Lee, E.; Sheldon, M.; Son, D. H. Exciton-to-Dopant Energy Transfer in Mn-Doped Cesium Lead Halide Perovskite Nanocrystals. *Nano Lett.* **2016,** *16*, 7376-7380.

50. Liu, W.; Lin, Q.; Li, H.; Wu, K.; Robel, I.; Pietryga, J. M.; Klimov, V. I. Mn^{2+}-Doped Lead Halide Perovskite Nanocrystals with Dual-Color Emission Controlled by Halide Content. *J. Am. Chem. Soc.* **2016,** *138*, 14954-14961.

51. Guria, A. K.; Dutta, S. K.; Adhikari, S. D.; Pradhan, N. Doping Mn^{2+} in Lead Halide Perovskite Nanocrystals: Successes and Challenges. *ACS Energy Lett.* **2017,** *2*, 1014-1021.

52. Hu, Q.; Li, Z.; Tan, Z.; Song, H.; Ge, C.; Niu, G.; Han, J.; Tang, J. Rare Earth Ion- Doped $CsPbBr_3$ Nanocrystals. *Adv. Opt. Mater.* **2018,** *6*, 1700864.

53. Song, E.; Ding, S.; Wu, M.; Ye, S.; Chen, Z.; Ma, Y.; Zhang, Q. Tunable White Upconversion Luminescence from Yb^{3+}-Tm^{3+}-Mn^{2+} Tri-Doped Perovskite Nanocrystals. *Opt. Mater. Express* **2014,** *4*, 1186-1196.

54. Pan, G.; Bai, X.; Yang, D.; Chen, X.; Jing, P.; Qu, S.; Zhang, L.; Zhou, D.; Zhu, J.; Xu, W.*; et al.* Doping Lanthanide into Perovskite Nanocrystals: Highly Improved and Expanded Optical Properties. *Nano Lett.* **2017,** *17*, 8005-8011.

55. Mir, W. J.; Mahor, Y.; Lohar, A.; Jagadeeswararao, M.; Das, S.; Mahamuni, S.; Nag, A. Postsynthesis Doping of Mn and Yb into $CsPbX_3$ (X= Cl, Br, or I) Perovskite Nanocrystals for Downconversion Emission. *Chem. Mater.* **2018,** *30* (22), 8170-8178.

56. Wang, L.; Zhou, H.; Hu, J.; Huang, B.; Sun, M.; Dong, B.; Zheng, G.; Huang, Y.; Chen, Y.; Li, L.*; et al.* A Eu^{3+}-Eu^{2+} Ion Redox Shuttle Imparts Operational Durability to Pb-I Perovskite Solar Cells. *Science* **2019,** *363*, 265-270.

57. van der Stam, W.; Geuchies, J. J.; Altantzis, T.; van den Bos, K. H. W.; Meeldijk, J. D.; Van Aert, S.; Bals, S.; Vanmaekelbergh, D.; de Mello Donega, C. Highly Emissive Divalent-Ion-Doped Colloidal $CsPb_{1-x}M_xBr_3$ Perovskite Nanocrystals through Cation Exchange. *J. Am. Chem. Soc.* **2017,** *139*, 4087-4097.

58. Zou, S.; Liu, Y.; Li, J.; Liu, C.; Feng, R.; Jiang, F.; Li, Y.; Song, J.; Zeng, H.; Hong, M.*; et al.* Stabilizing Cesium Lead Halide Perovskite Lattice through Mn(II) Substitution for Air-Stable Light-Emitting Diodes. *J. Am. Chem. Soc.* **2017,** *139*, 11443-11450.

59. Begum, R.; Parida, M. R.; Abdelhady, A. L.; Murali, B.; Alyami, N. M.; Ahmed, G. H.; Hedhili, M. N.; Bakr, O. M.; Mohammed, O. F. Engineering Interfacial Charge Transfer in $CsPbBr_3$ Perovskite Nanocrystals by Heterovalent Doping. *J. Am. Chem. Soc.* **2017,** *139*, 731-737.

60. Milstein, T. J.; Kroupa, D. M.; Gamelin, D. R. Picosecond Quantum Cutting Generates Photoluminescence Quantum Yields Over 100% in Ytterbium-Doped $CsPbCl_3$ Nanocrystals. *Nano Lett.* **2018,** *18*, 3792-3799.

61. Yong, Z.-J.; Guo, S.-Q.; Ma, J.-P.; Zhang, J.-Y.; Li, Z.-Y.; Chen, Y.-M.; Zhang, B.-B.; Zhou, Y.; Shu, J.; Gu, J.-L.*; et al.* Doping-Enhanced Short-Range Order of Perovskite Nanocrystals for Near-Unity Violet Luminescence Quantum Yield. *J. Am. Chem. Soc.* **2018,** *140*, 9942-9951.

62. Bi, C.; Wang, S.; Li, Q.; Kershaw, S. V.; Tian, J.; Rogach, A. L. Thermally Stable Copper(II)-Doped Cesium Lead Halide Perovskite Quantum Dots with Strong Blue Emission. *J. Phys. Chem. Lett.* **2019**, 943-952.

63. Woo, J. Y.; Kim, Y.; Bae, J.; Kim, T. G.; Kim, J. W.; Lee, D. C.; Jeong, S. Highly Stable Cesium Lead Halide Perovskite Nanocrystals through in Situ Lead Halide Inorganic Passivation. *Chem. Mater.* **2017,** *29*, 7088-7092.

64. Shen, X.; Zhang, Y.; Kershaw, S. V.; Li, T.; Wang, C.; Zhang, X.; Wang, W.; Li, D.; Wang, Y.; Lu, M.*; et al.* Zn-Alloyed CsPbI$_3$ Nanocrystals for Highly Efficient Perovskite Light-Emitting Devices. *Nano Lett.* **2019**, DOI: 10.1021/acs.nanolett.8b04339.

65. Mondal, N.; De, A.; Samanta, A. Achieving Near-Unity Photoluminescence Efficiency for Blue-Violet-Emitting Perovskite Nanocrystals. *ACS Energy Lett.* **2019,** *4*, 32-39.

66. Ball, J. M.; Petrozza, A. Defects in Perovskite-Halides and Their Effects in Solar Cells. *Nat. Energy* **2016,** *1*, 16149.

67. Nayak, P. K.; Sendner, M.; Wenger, B.; Wang, Z.; Sharma, K.; Ramadan, A. J.; Lovrinčić, R.; Pucci, A.; Madhu, P. K.; Snaith, H. J. Impact of Bi^{3+} Heterovalent Doping in Organic–Inorganic Metal Halide Perovskite Crystals. *J. Am. Chem. Soc.* **2018,** *140*, 574-577.

68. Lozhkina, O. A.; Murashkina, A. A.; Shilovskikh, V. V.; Kapitonov, Y. V.; Ryabchuk, V. K.; Emeline, A. V.; Miyasaka, T. Invalidity of Band-Gap Engineering Concept for Bi^{3+} Heterovalent Doping in CsPbBr$_3$ Halide Perovskite. *J. Phys. Chem. Lett.* **2018,** *9*, 5408-5411.

69. Yao, J.-S.; Ge, J.; Han, B.-N.; Wang, K.-H.; Yao, H.-B.; Yu, H.-L.; Li, J.-H.; Zhu, B.-S.; Song, J.-Z.; Chen, C.*; et al.* Ce^{3+}-Doping to Modulate Photoluminescence Kinetics for Efficient CsPbBr$_3$ Nanocrystals Based Light-Emitting Diodes. *J. Am. Chem. Soc.* **2018,** *140*, 3626-3634.

70. Yin, J.; Ahmed, G. H.; Bakr, O. M.; Brédas, J.-L.; Mohammed, O. F. Unlocking the Effect of Trivalent Metal Doping in All-Inorganic CsPbBr$_3$ Perovskite. *ACS Energy Lett.* **2019**, 789-795.

71. Di Stasio, F.; Christodoulou, S.; Huo, N.; Konstantatos, G. Near-Unity Photoluminescence Quantum Yield in CsPbBr$_3$ Nanocrystal Solid-State Films via Postsynthesis Treatment with Lead Bromide. *Chem. Mater.* **2017,** *29*, 7663-7667.

72. Li, F.; Liu, Y.; Wang, H.; Zhan, Q.; Liu, Q.; Xia, Z. Postsynthetic Surface Trap Removal of CsPbX$_3$ (X = Cl, Br, or I) Quantum Dots via a ZnX$_2$/Hexane Solution toward an Enhanced Luminescence Quantum Yield. *Chem. Mater.* **2018,** *30*, 8546-8554.

73. Abdi-Jalebi, M.; Andaji-Garmaroudi, Z.; Cacovich, S.; Stavrakas, C.; Philippe, B.; Richter, J. M.; Alsari, M.; Booker, E. P.; Hutter, E. M.; Pearson, A. J.*; et al.* Maximizing and Stabilizing Luminescence from Halide Perovskites with Potassium Passivation. *Nature* **2018,** *555*, 497.

74. Ahmed, G. H.; El-Demellawi, J. K.; Yin, J.; Pan, J.; Velusamy, D. B.; Hedhili, M. N.; Alarousu, E.; Bakr, O. M.; Alshareef, H. N.; Mohammed, O. F. Giant Photoluminescence Enhancement in CsPbCl$_3$ Perovskite Nanocrystals by Simultaneous Dual-Surface Passivation. *ACS Energy Lett.* **2018,** *3*, 2301-2307.

75. Lu, M.; Zhang, X.; Zhang, Y.; Guo, J.; Shen, X.; Yu, W. W.; Rogach, A. L. Simultaneous Strontium Doping and Chlorine Surface Passivation Improve Luminescence Intensity and Stability of CsPbI$_3$ Nanocrystals Enabling Efficient Light-Emitting Devices. *Adv. Mater.* **2018,** *30*, 1804691.

76. Ke, W.; Xiao, C.; Wang, C.; Saparov, B.; Duan, H. S.; Zhao, D.; Xiao, Z.; Schulz, P.; Harvey, S. P.; Liao, W. Employing Lead Thiocyanate Additive to Reduce the Hysteresis and Boost the Fill Factor of Planar Perovskite Solar Cells. *Adv. Mater.* **2016,** *28*, 5214-5221.

77. Chiang, Y.-H.; Li, M.-H.; Cheng, H.-M.; Shen, P.-S.; Chen, P. Mixed Cation Thiocyanate-Based Pseudohalide Perovskite Solar Cells with High Efficiency and Stability. *ACS Appl. Mater. Interfaces* **2017,** *9*, 2403-2409.

78. Jiang, Q.; Rebollar, D.; Gong, J.; Piacentino, E. L.; Zheng, C.; Xu, T. Pseudohalide- Induced Moisture Tolerance in Perovskite $CH_3NH_3Pb(SCN)_2I$ Thin Films. *Angew. Chem., Int. Ed.* **2015,** *54*, 7617-7620.

79. Yu, Y.; Wang, C.; Grice, C. R.; Shrestha, N.; Chen, J.; Zhao, D.; Liao, W.; Cimaroli, A. J.; Roland, P. J.; Ellingson, R. J. Improving the Performance of Formamidinium and Cesium Lead Triiodide Perovskite Solar Cells Using Lead Thiocyanate Additives. *ChemSusChem* **2016,** *9*, 3288-3297.

80. Yu, Y.; Wang, C.; Grice, C. R.; Shrestha, N.; Zhao, D.; Liao, W.; Guan, L.; Awni, R. A.; Meng, W.; Cimaroli, A. J. Synergistic Effects of Lead Thiocyanate Additive and Solvent Annealing on the Performance of Wide-Bandgap Perovskite Solar Cells. *ACS Energy Lett.* **2017,** *2*, 1177-1182.

81. Pham, N. D.; Tiong, V. T.; Yao, D.; Martens, W.; Guerrero, A.; Bisquert, J.; Wang, H. Guanidinium Thiocyanate Selective Ostwald Ripening Induced Large Grain for High Performance Perovskite Solar Cells. *Nano Energy* **2017,** *41*, 476-487.

82. Koscher, B. A.; Swabeck, J. K.; Bronstein, N. D.; Alivisatos, A. P. Essentially Trap-Free $CsPbBr_3$ Colloidal Nanocrystals by Postsynthetic Thiocyanate Surface Treatment. *J. Am. Chem. Soc.* **2017,** *139*, 6566-6569.

83. Leng, M.; Yang, Y.; Chen, Z.; Gao, W.; Zhang, J.; Niu, G.; Li, D.; Song, H.; Zhang, J.; Jin, S.*; et al.* Surface Passivation of Bismuth-Based Perovskite Variant Quantum Dots To Achieve Efficient Blue Emission. *Nano Lett.* **2018,** *18*, 6076-6083.

84. Behera, R. K.; Das Adhikari, S.; Dutta, S. K.; Dutta, A.; Pradhan, N. Blue-Emitting $CsPbCl_3$ Nanocrystals: Impact of Surface Passivation for Unprecedented Enhancement and Loss of Optical Emission. *J. Phys. Chem. Lett.* **2018,** *9*, 6884-6891.

85. Wu, Y.; Wei, C.; Li, X.; Li, Y.; Qiu, S.; Shen, W.; Cai, B.; Sun, Z.; Yang, D.; Deng, Z.*; et al.* In Situ Passivation of $PbBr_6^{4-}$ Octahedra toward Blue Luminescent $CsPbBr_3$ Nanoplatelets with Near 100% Absolute Quantum Yield. *ACS Energy Lett.* **2018,** *3*, 2030-2037.

86. Reiss, P.; Protière, M.; Li, L. Core/Shell Semiconductor Nanocrystals. *Small* **2009,** *5*, 154-168.

87. Sun, C.; Zhang, Y.; Ruan, C.; Yin, C.; Wang, X.; Wang, Y.; Yu, W. W. Efficient and Stable White LEDs with Silica-Coated Inorganic Perovskite Quantum Dots. *Adv. Mater.* **2016,** *28*, 10088-10094.

88. Xu, K.; Lin, C. C.; Xie, X.; Meijerink, A. Efficient and Stable Luminescence from Mn^{2+} in Core and Core–Isocrystalline Shell $CsPbCl_3$ Perovskite Nanocrystals. *Chem. Mater.* **2017,** *29*, 4265-4272.

89. Ma, J.-P.; Chen, Y.-M.; Zhang, L.-M.; Guo, S.-Q.; Liu, J.-D.; Li, H.; Ye, B.-J.; Li, Z.-Y.; Zhou, Y.; Zhang, B.-B.*; et al.* Insights into the Local Structure of Dopants, Doping Efficiency, and Luminescence Properties of Lanthanide-Doped $CsPbCl_3$ Perovskite Nanocrystals. *J. Mater. Chem. C* **2019,** *7*, 3037-3048.